VALIDATION OF AN ELECTROMAGNETIC INDUCTION SIMULATION FOR DEFECTS DETECTION: A QUASI-STATIC MODEL FOR AN AUTOMATED INSPECTION SYSTEM

Fernandez-Perez Nora, Gamallo-Ponte Pablo

Inspiralia Tecnologias Avanzadas SL, Calle Estrada 10-B, 28034 Madrid, Spain

Abstract

The herein presented paper describes the simulation carried out in the scope of defects detection through electromagnetic induction and the validation with experimental test. A coupled electromagnetic and thermal model was carried out with the software ANSYS Multhyphysics. Through this method the possibility to detect defects based in electromagnetic induction was assessed. In fact detection occurs due to the induced current concentration on the edges of the defects and thus they can be visible in the resulting induced current patterns as well as on the generated temperatures. In addition a quasi-static model was developed for replicating a system in which the defects tool is moving for a completely automatized inspection. An experimental test was also performed for the validation of this predictive tool, to finally obtain a reliable and consistent model that may be used for future studies. This paper demonstrates the accuracy and match of the results between the simulation model and the physical experiment and thus the availability of the model to optimize the system and required parameters, prior to the physical construction and tests, with the consequent time and economic savings.

Key words: *induction heating, electro-thermal modeling, numerical simulation, experimental validation, mechanical design, engineering*

1 INTRODUCTION

Simulation tools for the analysis and design of electromagnetic systems (alone or coupled with other physics) is still reduced in industrial applications, mainly due to the following reasons: the complexity of simulating coupled non-linear and three-dimensional problems and the need of high performance computers. However in the last years much effort has being concentrated in solving electromagnetic problems (1) (2). The reason might lie in the increasingly use of electromagnetic systems for induction heating applications. In fact, induction heating provides many advantages compared to traditional heating processes (gas furnaces, etc.), mainly: a fast heating rate, well-defined heating locations, good reproducibility and low energy consumption, reduction of start-up and shutdown timing, low equipment and labour cost and low carbon footprint (3).

Electromagnetic Induction heating is based on the phenomenon by which an alternative current flowing through a coil induces a magnetic field and the subsequent eddy currents on an electrically conductive target part (workpiece). These eddy currents heat up the target workpiece due to the Joule effect. Thus, the heating pattern will be very closely related to the geometry of the target and the path of the coil, but also to other issues such as the skin effect (penetration of the currents below the piece surface), proximity and slot effects intrinsically related to the induction electromagnetic phenomena (4). In fact, these effects are those typically causing the non-uniform heating of magnetic pieces. In fact, no uniform currents are induced through the workpiece and the heat generation is concentrated on the surface.

This paper studies the heating and temperature distribution caused by an induction system through the Finite Element Method (FEM). A validation process is also performed to assess the accuracy of the tool to replicate such systems. The goal is then to obtain a reliable tool that serves to predict the behaviour of the system and to ultimately achieve the required parameters for which the induced current concentration will be the highest, prior to the physical construction and testing. Thus this work consists of two parts. In the first part, the numerical method and the experimental test are described in which the generator parameters (power and frequency), the coil-piece disposition, coil geometry (path,

dimensions and location), are replicated. In the second part the assessment about the reliability and accuracy of the simulation method, which couples electromagnetism and heat transfer, was studied by comparing simulation results with empirical data. For this purpose, the computed temperature distributions were analysed in both systems.

2 MATHEMATICAL MODEL AND SIMULATION METHOD

In this section the equations for modelling the heat induction process are introduced; on the one hand, the electromagnetic and on the other the heat transfer equations are presented. The simulation method implemented is based on the numerical solution of these mathematical equations by means of the finite element method.

2.1 Electromagnetic model

The electromagnetic fields in matter obey the so-called macroscopic Maxwell's equations. These equations relate the electromagnetic fields: electric field $\vec{E}$, the displacement field $\vec{D}$, the magnetic flux density $\vec{B}$, the magnetic field intensity $\vec{H}$, the free current density $\vec{J}_f$, and the free electric charge density ρ_f . The free charge and current refer to those not associated with matter (dielectric and/or magnetic materials).

For general time-varying electromagnetic fields, the Maxwell equations in differential form can be written as (5):

$\nabla \times \vec{H} = \overrightarrow{J_f} + \frac{\partial \vec{D}}{\partial t}$, Ampere's law (with Maxwell addition)

$\nabla \times \vec{E} = -\frac{\partial \vec{B}}{\partial t}$, Faraday's law

$\nabla \cdot \vec{B} = 0$, Gauss's law for magnetism

$\nabla \cdot \vec{D} = \rho_f$, Gauss's law

These equations have to be complemented with the continuity equation (charge conservation)

$$\nabla \cdot \vec{J}_f = -\frac{\partial \rho_f}{\partial t},$$

and the corresponding constitutive equations of each material:

$$\vec{D} = \vec{D}(\vec{E}), \qquad \vec{H} = \vec{H}(\vec{B})$$

The materials analysed in this work can be considered as linear, isotropic and homogeneous

$$\vec{D} = \varepsilon_r \varepsilon_0 \vec{E}, \qquad \vec{H} = \frac{\vec{B}}{\mu_r \mu_0}$$

where ε_0 is the vacuum permittivity and μ_0 the vacuum permeability and ε_r and μ_r the corresponding material relative permittivity and permeability.

For the electrical conductive materials holds

$\vec{J}_\sigma = \sigma \vec{E}$, Ohm's law

where σ is the material electric conductivity.

Since alternating (harmonic) input currents (voltages) are considered, under the previous assumptions, the steady-state harmonic fields will have the following form in complex notation:

$$F(x,t) = Re\left[e^{i\omega t}\hat{F}(x)\right]$$

where t represents time, x is the position, $\omega = 2\pi f$ is the angular frequency of the input current, i the imaginary unit number and $\hat{F}(x)$is the complex amplitude of the field.

The induction systems used in industry for heating process work in the so-called low-frequency regime. For low-frequency, the term in Ampere's law including the electric displacement can be neglected and the Maxwell's equations reduce to the so-called harmonic eddy current model:

$$\nabla \times \vec{B} = \mu_r \mu_0 \vec{J}_f$$

$$i\omega\vec{B} + \nabla \times \vec{E} = 0$$

$$\nabla \cdot \vec{B} = 0$$

$$\nabla \cdot \vec{E} = 0$$

The current I set to flow along the inductor coil is related to the current density $\vec{J}_f$ through the equation

$$I = \int_S \vec{J}_f \, d\vec{S}$$

where S is the coil cross section.

2.1.1 Finite Element Model. Mesh and skin effect

This set of equations can be discretized with the Finite Element Model, as implemented in the ANSYS® Emag software (6) (7), to solve them numerically. The outputs of these electromagnetic simulations are the generated electromagnetic fields and the induced eddy currents.

In order to ensure a good accuracy of the FEM simulations, it is crucial that the finite element mesh is characterized by a refined element size on the surface of the workpiece to represent properly the aforementioned skin effect. This is a very significant effect to take into account to achieve a reliable model, since the eddy currents will be concentrated on the surface of the part and thus, the FEM should include more than one element within the skin depth δ. Fortunately, the thickness of the skin depth can be estimated accurately from the following relation:

$$\delta = \sqrt{\frac{2}{\omega\sigma\mu_r\mu_o}}$$

On the other hand, in order to represent in the FEM model the 'unbounded' air surrounding the system, a finite size air box enclosing the workpiece and the inductor with suitable boundary conditions (magnetic flux tangential to its faces) was considered.

With regard to the coil, it is treated as a source conductor with a given current (provided by the generator) and hence a current intensity is introduced from one end of the coil and a ground (zero) voltage is set on the other end.

Since the electromagnetic transient period, previous to the steady-state harmonic regime, is very short in time and can be neglected, the initial conditions have no influence and therefore are not required in the numerical model.

2.2 Heat transfer model

The electromagnetic model must be coupled with the heat transfer problem, to study the thermal effects of the induction phenomena. The following equations will guide the thermal behaviour, which varies depending on the element location: inside de model (conduction effects) or in the exterior surface (which accounts for conduction, radiation and convection effects).

$\rho \cdot c \frac{\partial T}{\partial t} = k \cdot \nabla^2 T + Q_{induction}$, condition inside

$\rho \cdot c \frac{\partial T}{\partial t} = k \cdot \nabla^2 T + Q_{induction} - A \cdot \sigma \cdot \varepsilon \cdot F \cdot \left(T^4 - {T_{air}}^4\right) - A \cdot h \cdot (T - T_{air})$, condition on the surface

The heat generated in the materials by the electric currents due to the Joule effect is included as a heat source in the heat conductive equation:

$$\rho c \frac{\partial T}{\partial t} - \nabla \cdot (k \nabla T) = \frac{|J|^2}{2\sigma}$$

where T is the temperature and ρ, c and k the material density, specific heat and thermal conductivity, respectively.

The boundary conditions of the heat transfer problem consider the Newton's law of cooling with an effective heat transfer coefficient h in the exterior surfaces of the pieces, to account for heat losses/gains $\dot{q}_{\text{ext}}$ from convection and radiation (linearized) with the surrounding media (air in our study).

$$\dot{q}_{\text{ext}} = h\,(T - T_{\text{air}})$$

The numerical solution of the thermal problem is performed by means of the Finite Element discretization (8) of the above heat transfer equation as implemented in ANSYS® Mechanical APDL. Assuming that the variation of the electromagnetic properties (ε_r μ_T , ε_T , σ $\mu_r, \varepsilon_r, \sigma$) with temperature is negligible, the coupling between the electromagnetic and thermal models reduces to a one-way, that is, the harmonic EM problem is solved first to compute the heat source produced by the Joule effect and this heat will be the input in the transient heat transfer problem.

3 NUMERICAL AND EMPIRICAL MODELS

In this section the model developed is described. The system for the experimental test was replicated through simulation and both characteristics are shown here. First the simulation of the induction heating is presented, which was implemented in the FEM software ANSYS® APDL.

3.1 Description of the numerical model

In this section the details of the validated model are provided, with the geometry, boundary conditions and the mesh details. The implemented method, consists on a metallic plate (workpiece) exposed to an electromagnetic induction field generated by a cooper coil (inductor) positioned above it (**Figure 1**). The coil and plate relative displacement velocity was 62.5 mm/s (Figure 1). The numerical model developed is based on a quasi-static model, to include the displacement of the tool with respect to the induction coil.

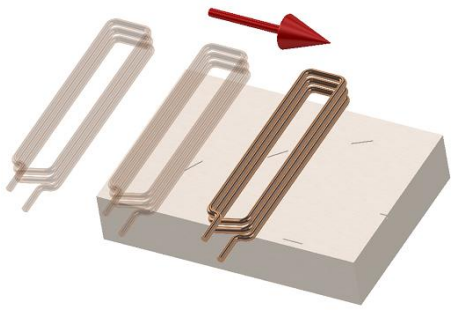


Figure 1. Geometry for numerical model. Coil and Plate with relative displacement

3.1.1 Geometry

In the following picture the plate dimensions used for the validation study and performed cracks can be seen. For simplification purposes and in order to reduce computational time, only a piece of 200mm has been considered. The plate and cracks dimension details are given in the following image.

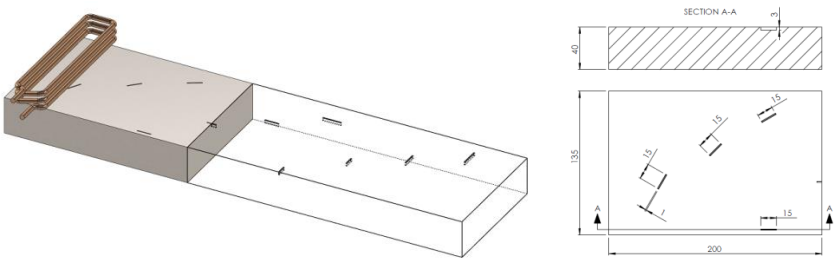


Figure 2. Entire configuration (left) and the part to be used on the study (right)

Coil dimensions details are given in the following picture:

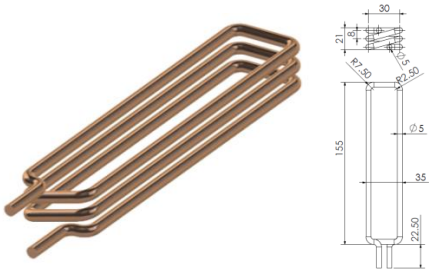


Figure 3. Coil dimensions

3.1.2 Properties and Boundary conditions

In this section the material properties and boundary conditions of the model are described. First the required parts to perform the electromagnetic simulation are mentioned, which comprise the assembly of the model that require the steel plate, the coil and the surrounding air, as demonstrated in the following figure.

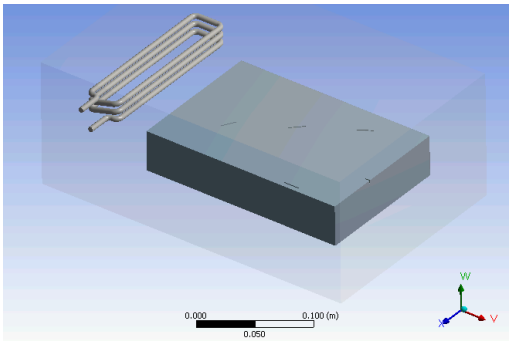


Figure 4. Simulation model. Air, Coil and Plate

The materials utilized and the most important properties related to the physics of the problem are presented here.

Table 1. Material properties

	ρ (kg/m3)	Cp (J/kg K)	K (W/m K)	ρ_{el} (ohm m)	μ_{rel}
AIR	1.2	1004	0.0257	-	1
STEEL	7850	486	51.9	$1.17e^{-7}$	5000
COPPER	8300	385	401	$1.7e^{-8}$	1

The conditions that were imposed over the electromagnetic model are:

1. A magnetic flux boundary condition which imposes a constraint on the direction of the magnetic flux was imposed. This feature constraints the flux to be tangential and thus it must be applied to the exterior faces of the air and thus contain the magnetic flux inside the domain.
2. The coil was treated as a source conductor and thus the current was set on the inlet side of the coil. A zero ground voltage was set on the other end.

The electromagnetic problem was solved with a harmonic FEM study, in which the introduced frequency was 230 kHz. In the heat transient problem the boundary and initial conditions were the following:

1. Initial ambient temperature was set to 20° C.
2. Adiabatic conditions were set to the plate (No convection neither radiation was considered due to the reduced time pulse at which it will run and the fact that the heat will be mostly conducted through the plate).
3. The joule heat source obtained from the electromagnetic model was applied to the plate. For each coil position, the heat generation is loaded on the plate, with the previous temperatures as the initial condition.

Thus and to summarize the input parameters and some properties of the model are presented here:

Table 2. Model properties and boundary conditions

Parameter	**Value**
Current	252A
Frequency	230kHz
Power	4kW
T_{amb}	20ºC
Coil length	1070mm
Coil-piece distance	3mm

The Finite Element mesh used for the simulations is shown in **Figure 5**. As stated previously, a local mesh refinement was required close to the surface of the workpiece to ensure to simulate accurately the skin effect. Electromagnetic studies require a fine mesh, especially on the surface where the eddy

current will mostly take place, i.e. the skin depth (9). Due to this phenomenon, it is recommended that at least two elements are set within this depth to gather the eddy current properly. Considering the aforementioned magnetic properties (

Table **1**), the frequency of 230 kHz, the skin depth will be 5,07 μm.

With the aim of achieving more accurate results, an inflation of 5 layers was modelled and the first layer was set to 2μm as shown in the following figure.

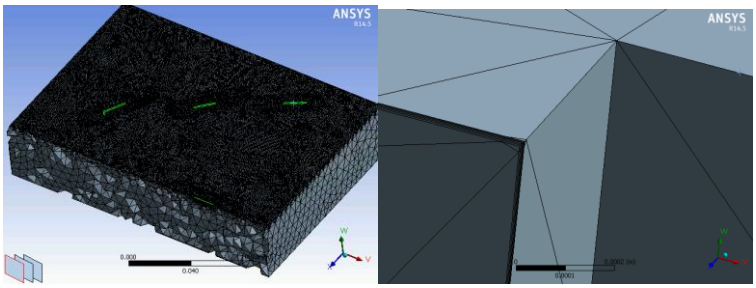


Figure 5. Model mesh (left) Skin depth layer's detail (right)

This study requires to be extremely careful with the mesh, since it must maintain the same mesh and nodal numbering in the plate, for transferring the nodal heat generation results obtained on the electromagnetic study to the transient thermal problem.

In the simulation, a first run of this model was carried out to obtain the electrical impedance $Z = V / I$ $Z = V/I$, of the system. Once the impedance is known, the current is set to match the actual prescribed power used for each particular experimental setting. From the phase (argument) of this impedance Z the capacity of the oscillator can be calculated (8.09μF), which required for the matching of the electrical circuit so that the voltage and current coming from the generator are in phase and thus, there is no reactive power.

In the FEM model of the transient heat transfer problem, the source terms and boundary conditions implemented were: the heat source (Joule Heating) coming from the previous solution of the electromagnetic problem and the heat losses through the workpiece surface represented by means of a heat transfer coefficient h. As initial condition, the coil and workpiece are assumed at room temperature (20.6 °C).

These calculations were done for a sequence of time steps, in which the coil was displaced, based on the velocity of the workpiece movement (**Figure 1**).

3.2 Experimental test

This validation becomes crucial to assess the reliability of the numerical model for electromagnetic induction heating calculations and its feasibility as a design tool. To this aim, the temperature patterns of both, experimental and simulation results were compared at different time steps during the induction heating process.

The results of the temperatures generated by the induced current, were captured by a thermographic camera in a given time step, once the heating and the induction effects started. The images obtained by the camera are given in a sequence of x radial line of pixels at small time steps, as the plate displaces. Thus the image composition will comprise the sequence of these captured radial pixels (Figure 6).

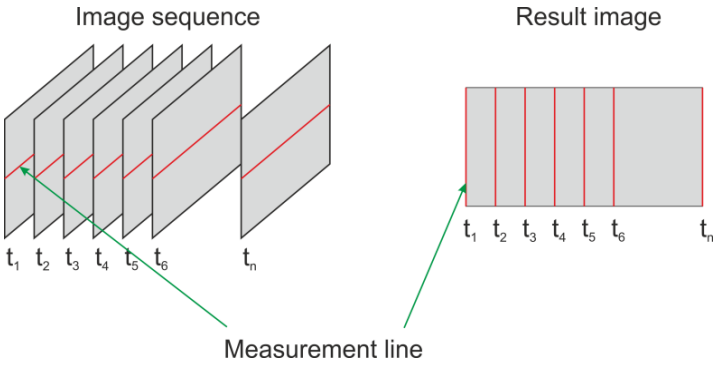


Figure 6. Image sequence and composition

Those digital output images were translated into a pc, for pre-processing and first results analyses were obtained (Figure 7). In fact the performed test, helped also to understand and evaluate the integration between the different components, comprising hardware, software and the control system in order to achieve a final image with the captured sequences from the camera, while the piece displacement is automatically carried out and controlled.

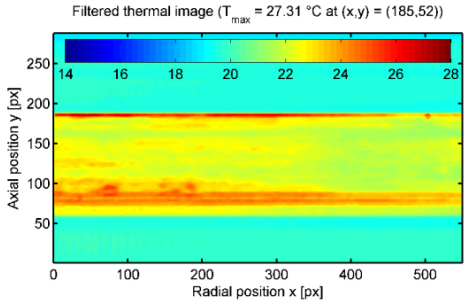


Figure 7. Processed first thermal gradient images

4 RESULTS AND VALIDATION

In this section the validation of the simulation method with experimental tests is demonstrated. The data that will be used for this purpose are temperatures patterns. The most relevant time step images are shown below. The position of the coil with respect to the plate was defined by the distance from the end of the coil to the plate (Figure 8), which will correspond to the different time steps, considering the initial position in which the distance is 25mm and thus t=0.

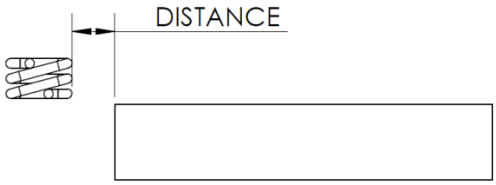


Figure 8. Distance between Coil and Plate

In the following images the temperature patterns at the first time steps can be observed:

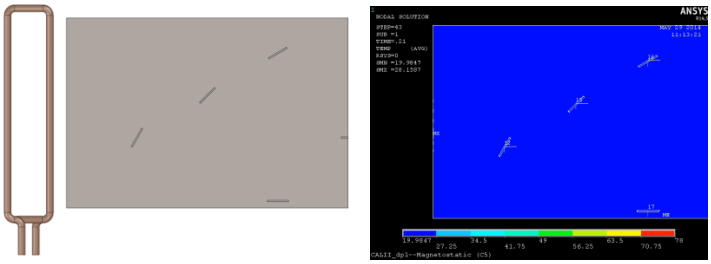


Figure 9. Model (top) and temperature pattern (bottom) at t=0.21 s, d=9.38mm

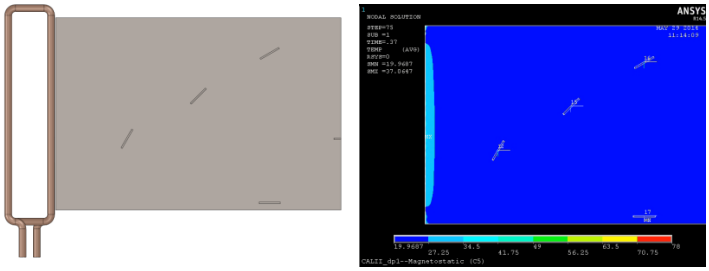


Figure 10. Model (Top) and temperature pattern (bottom) on surface. t=0.37s, d=0.63mm

Now the temperatures at different time steps are shown, in which the thermal distribution around the crack is observed. Those in which the coil is right above the crack is that corresponding to the 1.1-1.2s time step. The position in which the crack will be in the middle of the two wire coils is at 1.4s, as shown in the following images.

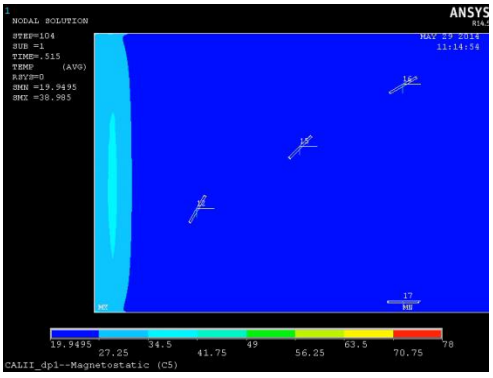


Figure 11. Temperature on surface. t=0.51s

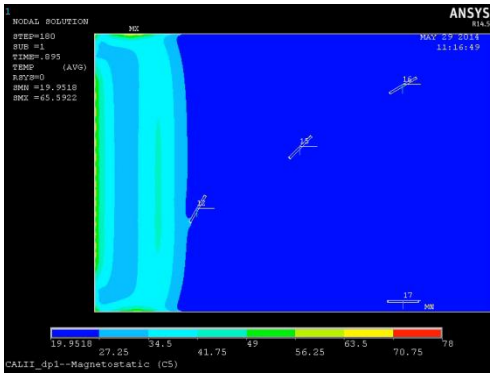


Figure 12. Temperature on surface. t=0.89s

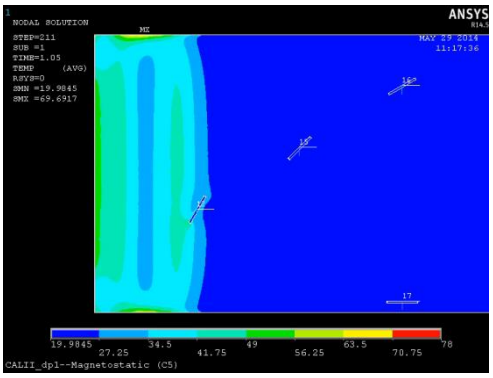


Figure 13. Temperature on surface. t=1.05s

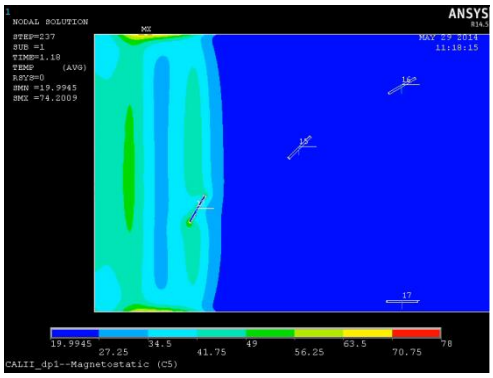


Figure 14. Temperature on surface. t=1.18s

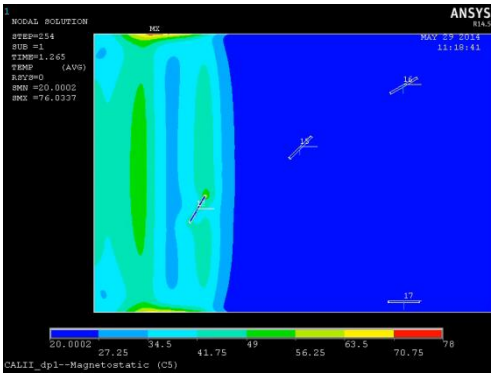


Figure 15. Temperature on surface. t=1.26s

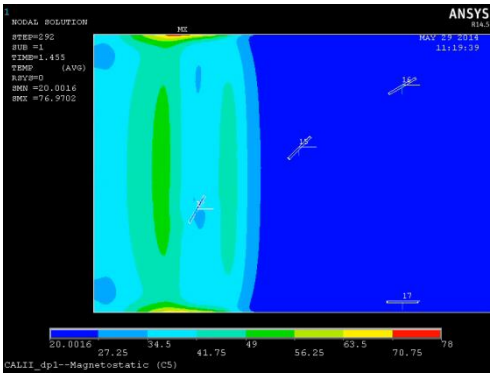


Figure 16. Temperature on surface. t=1.45s

General temperatures between 27°C and 49°C are found on the piece. The maximum temperature is found at the edges of the plate, due to the edge effect (9). These are very high also due to the coil winding which is positioned just above the ends of the plate.

Right under the coil temperatures around 45-49°C are found, instead between the coils 27-30°C are observed. Thus when the coil is positioned above the crack it will be highly visible, above all on the tips, due to the discontinuity that is generated on the induced current. However this effect will not to be captured by the camera since the coil covers the crack from this top perspective.

In the following images the experimental test results, obtained from the thermographic camera are compared with the simulation results. The accessible images from the camera are based on a grey scale map of bits (based on digital unit values) that can be translated to temperature differences. For this reason first the thermal differences were compared and then also those were traduced into temperatures (within a color scale map) considering an ambient temperature of 20°C, to be able to compare both results. In the following image first comparison of both images at the same time step (1.4s), in which the crack is between the coils are presented.

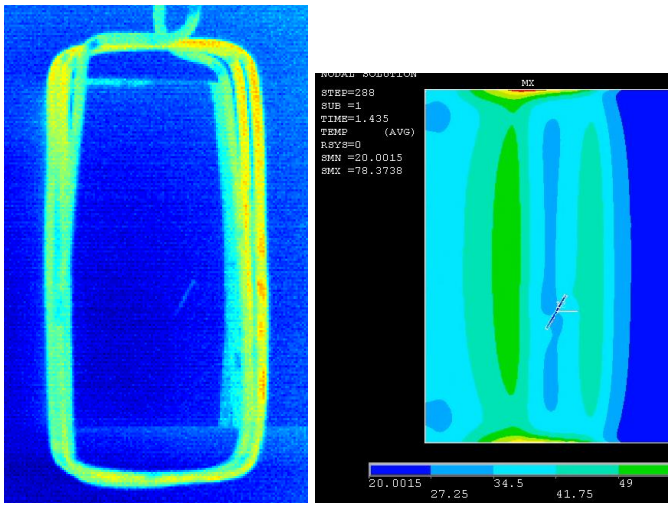


Figure 17. Initial comparison between a thermographic image and simulation results

As it can be observed the coil slightly differs from that used for the model. In fact the coil that was used for the real case, was bended manually, and thus it does not show equidistant spiral wires. In addition the diameter of the coil that was finally used for the experimental case was smaller than that defined for the simulation. However the main differences which are expected in this regard are related to the width and length between the coils. In the test the width and length is higher and this may lead to some differences on the results due to the following:

- The different position or distance between the coil and the crack, above all taken into account the rapid heat decrease that happens in a very short time.
- The coil winding will be a little displaced from the edges of the plate (Figure 17), and this may lead to lower temperatures than those found on the simulation.

However the goal of this comparison is to provide a qualitative validation and as observed below a very good agreement was achieved. In the following image the thermal difference between the crack and the surroundings was checked from the thermographic image.

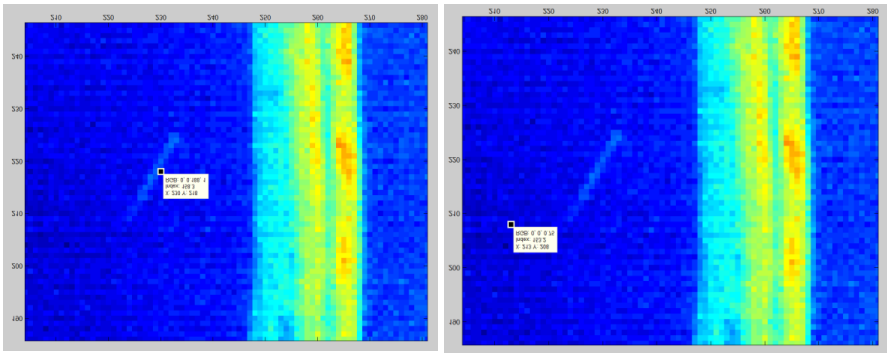


Figure 18. Digital unit values on the surroundings (left). On the edges (middle) and tips (right) of the crack

The values between those points, on the surface of the plate (left) and the middle of the crack (right) were compared and a thermal difference of 5-7°C was found from the surroundings to the middle of the crack. If those are compared to the results obtained from the simulation (Figure 19), we can

observe that the temperature jump between these two zones is around this value, 7°C (when the crack is positioned between the coils).

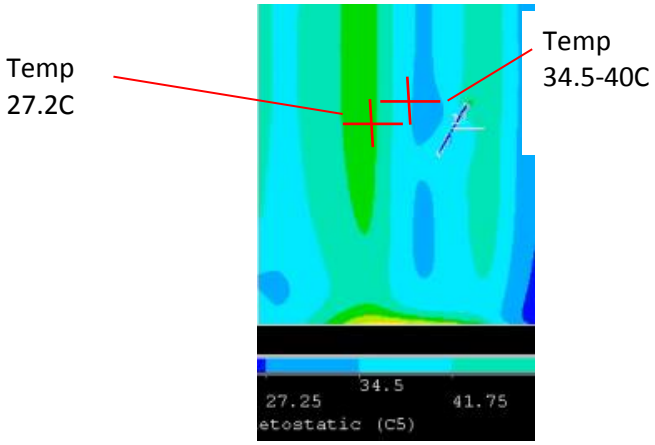


Figure 19. Simulation temperatures at the measurement points

When the digital units from the thermographic camera are translated to temperatures, considering an ambient temperature of 20C, the following values are obtained:

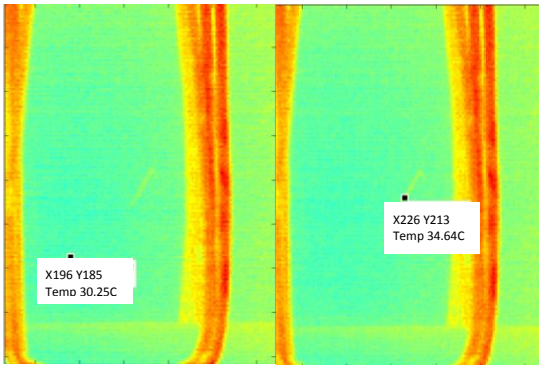


Figure 20. Temperatures from the thermographic images

Temperatures found around the crack are a 34°C, which match quite well with those obtained from the simulation, between 34-40°C (Figure 19). Thus for this general consideration of the temperatures and the qualitative validation purpose, a quite well match of temperatures was found, around 27-30°C in the surroundings between the coils of both the test and simulation and around 34-40°C on the cracks o near the edges of the crack.

This approximation was done considering that the results from the thermographic camera cannot be used to read the exact temperature, in a high extent due to the image noise, but an overall thermal map can be obtained as shown.

Hence, further details around the crack and tips of the crack are difficult to validate also due to the resolution or the camera and the fact that the sequence image composition, will not provide accurate temperatures from the IR maps. In fact this is the reason for which slightly higher temperatures are defining the crack and its geometry on the images from the thermographic camera (Figure 20) and instead lower temperatures on the simulation. The fact is that simulation provides also the temperatures inside de crack, on the plate deeper area and thus not only on the surface as it does the

camera. Thus the thermographic images renders that the IR signals from this deeper area are not received from the camera, and thus only the higher temperature of the edges will be received. A detailed view of the crack and its temperature patter is observed on the simulation image below, where the edges and near surroundings show the higher temperatures and a stronger IR signal, validating this assumption.

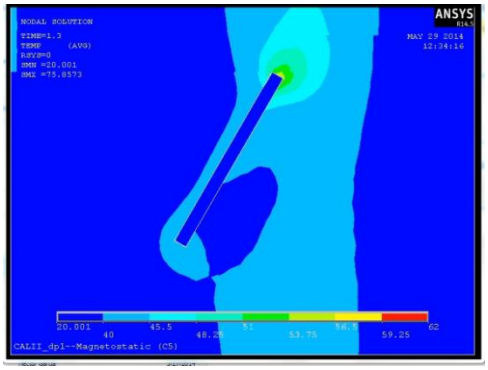


Figure 21. Detailed view of the crack

5 RESULTS AND CONCLUSIONS

A coupled electromagnetic and thermal simulation tool, based on the Finite Element Method, was implemented and validated against an experimental setup consisting of a plate with an induction coil moving above it. The accuracy of the simulation relies on the reliability and precision of the input data, mainly: materials properties (magnetic permeability, electric conductivity, permittivity, emissivity), the ambient temperature as well as the heat transfer coefficient (to carefully gauge the heat losses to the surrounding air by radiation and convection).

The performed comparison showed some slightly differences on the results due to the different position and shape of the configuration, mainly the coil, in the simulation and the real case. In any case the goal is to provide a qualitative validation and as observed very good agreement was achieved. Temperatures found around the crack are a 34°C, which match quite well with those obtained from the simulation (between 34-40°C). A quite well match of temperatures was also found in the surroundings between the coils of both the test and simulation, 27-30°C and 34-40°C on the cracks o near the edges of the crack. Further details around the crack and tips of the crack are difficult to validate also due to the resolution or the camera. In fact this is the reason for which slightly higher temperatures are defining the crack and its geometry on the images from the thermographic camera and instead lower temperatures on the simulation (simulation provides also the temperatures inside de crack, on the plate deeper area and thus not only on the surface as it does the camera). The thermographic images renders that the IR signals from this deeper area are not received from the camera, and thus only the higher temperature of the edges will be received.

Due to the good agreement between the measurements and the numerical results, the implemented simulation tool was considered suitable for performing the analysis of induction systems. The simulation was found to be a very powerful tool to check the system behavior saving time and resources.

ACKNOWLEDGMENTS

This work was carried out in the scope of the EU FP7 TRAINWHEELS project (grant agreement no: ID 603410).

REFERENCES

1. **Bermudez de Castro, Alfredo, Gomez, Dolores and Salgado, Pilar.** *Mathematical models and numerical simulation in electromagnetism.* s.l. : Springer, 2014.

2. *Large-Scale Electromagnetic Computation for Modeling and Applications.* **Qing Huo Liu, Lijun Jiang, Weng Cho Chiew.** 2, s.l. : IEEE, 2013, IEEE, Vol. 101.

3. **Davies, E.J.** *Conduction and Induction Heating.* London : Peregrinus, 1990.

4. **Rudney, Valery, et al., et al.** *Hand book of Induction Heating (Manufacturing Engineering and Materialas processing).* 2003.

5. **Cessenat, M.** *Mathematical methods in Electromagnetism.* s.l. : World Scientific, 1996.

6. **ANSYS Inc.** *Low Frequency Electromagnetic Analysis.* 2009.

7. —. *Coupled field analysis guide.* 2009.

8. **Zienkiewicz, O.C. and Taylor, R. L.** *The Finite Element Method.* s.l. : Butterworth-Heinemann, 2000.

9. **D2.1, Inspiralia.** *Deliverable 2.1. Computation of thermal maps for different configurations if induction system and cracks.* 2014.

10. **A. Bossavit.** *Computational Electromagnetism.* San Diego CA : Academis Press, 1998.

11. **D1.1, Inspiralia.** *Deliverable 1.1. Report on the geometrical and physical characterization of wheel-axles systems and the surface cracks to be detected.* Madrid : s.n., 2014.

12. *Thermal and magnetic field analysis of induction heating problems.* **Hiroki Kawaguchi, Masato Enokizono, Takashi Todaka.** 193–198, Oita, Japan : s.n., (2005), Vol. Journal of Materials Processing Technology 161 .

13. *Defect characterisation based on heat diffusion using induction thermography testing.* **Yunze He, Mengchun Pan and Feilu Luo.** 104702, Newcastle, United Kingdom : American Institute of Physics., 2012, Vol. REVIEW OF SCIENTIFIC INSTRUMENTS 83.

14. *Numerical analysis and thermographic investigation of induction heating.* **Matej Kranjc, Anze Zupanic, Damijan Miklavcic, Tomaz Jarm.** 3585–3591, Ljubljana, Slovenia : Elsevier, 2010, Vol. International Journal of Heat and Mass Transfer 53.

15. *2D finite element method study of the stimulation induction heating in synchronic thermography NDT.* **Madani Louaayou, Nasreddine Naït-Saïd, Fatima Zohra Louai.** 577–581, Saint-Nazaire, France : Elsevier, 2008, Vol. NDT&E International 41.

16. *Derivation of simplified formulas to predict deformations of plate in steel.* **Kang-Yul Bae, Young-Soo Yang, Chung-Min Hyun, Si-Hun Cho.** International Journal of Machine Tools & Manufacture 48 1646–1652, s.l. : Elsevier Ltd., 2008.

17. *A computer aided finite element/experimental analysis of induction heating process of steel.* **K. Sadeghipour, J.A. Dopkin, K. Li.** 195-205, Philadelphia : Elsevier, 1993, Vol. 28.

18. *Numerical and experimental thermal analysis for a metallic hollow cylinder subjected to step-wise electro-magnetic induction heating.* **Jiin-Yuh Jang, Yu-Wei Chiu.** 1883–1894, Tainan, Taiwan : Elsevier, 2006, Vol. Applied Thermal Engineering 27.

19. *MECHANISMS AND MODELS FOR CRACK DETECTION WITH INDUCTION THERMOGRAPHY.* **J. Vrana, M. Goldammer, J. Baumann, M. Rothenfusser, and W. Arnold.** CP975, s.l. : Review of Quantitative Nondestructive Evaluation. Ed. D. O. Thompson and D. E. Chimenti., 2008, Vol. 27.

20. **CEN.** UNE-EN_13262=2005+A2. *Aplicaciones Ferroviarias Ejes montados y boggies Ruedas. Requisitos del Producto.* s.l. : AENOR, 2011.

21. BS 5892-3. *Railway rolling stock materials — Part 3 Specification for monobloc wheels for traction and trailing stock.* s.l. : British Standard , 2006.

22. **Inspiralia.** *Deliverable 1.1. Report on the geometrical and physical characterization of wheel-axles systems and the surface cracks to be detected.* Madrid : s.n., 2014.

23. **Perez, Nora Fernandez.** *Validation of an electromagnetic induction simulation for defects detection: A quasi-static model for an automated inspection system.* 2015.